

FULL PAPER

Open Access



Coseismic changes in subsurface structure associated with the 2018 Hokkaido Eastern Iburi Earthquake detected using autocorrelation analysis of ambient seismic noise

Hiroki Ikeda^{1,2} and Ryota Takagi^{1*} 

Abstract

Autocorrelation analysis using ambient noise is a useful method to detect temporal changes in wave velocity and scattering property. In this study, we investigated the temporal changes in seismic wave velocity and scattering property in the focal region of the 2018 Hokkaido Eastern Iburi Earthquake. The autocorrelation function (ACF) was calculated by processing with bandpass filters to enhance 1–2 Hz frequency range, with aftershock removal, and applying the one-bit correlation technique. The stretching method was used to detect the seismic wave velocity change. After the mainshock, seismic velocity reductions were observed at many stations. At N.AMAH and ATSUMA, which are located close to the mainshock, we detected 2–3% decreases in seismic wave velocity. We compared parameters indicating strong ground motion and showed the possibility of correlations with peak dynamic strain and seismic velocity reduction. We also investigated the relationship between waveform correlation and lag time, using ACFs from before and after the mainshock, and detected distortion of the ACF waveform. The source of the waveform decorrelation was estimated to be located near the maximum coseismic slip, at around 30 km depth. Thus, distortion of the ACF waveform may reflect the formation of cracks, due to faulting at approximately 30 km depth.

Keywords: Seismic velocity changes, Ambient noise, Scatterer distribution change, Autocorrelation function, Hokkaido Eastern Iburi Earthquake, Seismic interferometry

Introduction

Earthquakes, and their genesis processes, change the internal state of the Earth, via stress state changes, pore fluid movement, fractures around the fault, and shallow ground damage. The Earth's interior state affects seismic wave velocity and scatterer distribution, or scattering properties. Therefore, we can understand the temporal evolution of the Earth's interior state, when associated with earthquakes, better, by monitoring changes in the seismic wave propagation process over time.

Seismic interferometry is a useful method with which to monitor temporal change in the seismic wave propagation process (e.g., Sens-Schönfelder and Wegler 2006). Seismic interferometry is a method to obtain Green's function between two seismic stations, by the computing cross-correlation functions of either ambient noise or coda waves. Repeating earthquakes and artificial explosions have also been used to detect seismic velocity changes associated with large earthquakes or volcanic activity (e.g., Nishimura et al. 2000; Poupinet et al. 1984). However, since repeating earthquakes do not occur frequently, and artificial explosions are expensive, the temporal and spatial resolution of velocity changes has been low in these studies. Methods using auto- and cross-correlation functions of the continuous ambient noise record (ACFs and CCFs) can estimate temporal changes

*Correspondence: ryota.takagi.c1@tohoku.ac.jp

¹ Research Center for Prediction of Earthquakes and Volcanic Eruptions, Graduate School of Science, Tohoku University, 6-6 Aza-Aoba, Aramaki, Aoba-ku, Sendai 980-8578, Japan

Full list of author information is available at the end of the article

in the velocity structure with better spatial and temporal resolution.

Several studies have reported temporal changes in the velocity structure associated with large earthquakes, by applying seismic interferometry (e.g., Brenguier et al. 2008; Wegler et al. 2009). Regarding the seismic velocity change which accompanied large earthquakes, damage to the shallow subsurface resulting from strong ground motion has been found to contribute largely to the velocity reduction of the near surface layer (e.g., Hobiger et al. 2016; Nakata and Snieder 2011; Sawazaki and Snieder 2013; Takagi et al. 2012). In addition to the damage in shallow, subsurface layers, deformation and stress relaxation in the deep crust associated with large earthquakes have also been reported to have caused seismic velocity drops—and their recovery—after earthquakes (Brenguier et al. 2008; Chen et al. 2010). Moreover, several studies have reported that seismic velocity changed during earthquake swarm activities and also during slow slip events that did not generate strong ground motion (Maeda et al. 2010; Ueno et al. 2012; Rivet et al. 2011).

Changes in subsurface scatterer distribution, and/or scattering property, can also be monitored with seismic interferometry. While seismic velocity changes cause phase shifts in the ACF and CCF waveforms, scattering property changes cause waveform shape changes, which can be measured through the reduced cross-correlation coefficient between waveforms measured before and after scattering property changes. Obermann et al. (2014) detected decreased correlation values between CCFs from before and after the 2008 Sichuan earthquake and located the area of the change in the scattering property near the fault zone. Chen et al. (2015) have reported changes to the repeating earthquake waveforms after the 1999 Chichi earthquake and attributed the changes to deep fault zone damage.

The M_{jma} 6.7 Hokkaido Eastern Iburi Earthquake occurred on September 6, 2018; it generated strong ground motion, with the maximum seismic intensity reaching 7, the highest value in the Japan Meteorological Agency (JMA) scale (<https://www.jma.go.jp/jma/en/Activities/inttable.html>). The JMA estimated the depth of the hypocenters at 37 km, which was deeper than normal for inland earthquakes in Japan. The average depth of the Moho discontinuity in the central part of the northeastern Japan arc is ~35 km (e.g., Katsumata 2010). Kita et al. (2010, 2012) have shown that the low-velocity anomaly zone corresponding to the seismic velocity of the crustal rock ($V_p < 7.2$ km/s and $V_s < 4.2$ km/s) existed for a depth of 35–80 km under the Hidaka district of Hokkaido. Because of the complicated structure, this earthquake may have occurred at a depth of 37 km. The initial focal mechanism solution determined by the polarization of

P-waves showed a strike-slip type fault, with a pressure axis extending from the northeast in a westerly direction to the southwest, whereas the centroid moment tensor solution showed a reverse fault type (National Research Institute for Earth Science and Disaster Resilience 2018)—a discrepancy which suggested a complex fault rupture process.

In the study reported here, we detected temporal change in subsurface structures during the 2018 Hokkaido Eastern Iburi Earthquake, based on ACF analysis, and using ambient noise records. We focused on temporal changes, not only in seismic velocity, but also in scattering property.

Data and methods

We computed ACFs for ambient noise and estimated temporal variations in seismic velocity according to the methods described in Yukutake et al. (2016), and Wegler et al. (2009). We used continuous, vertical-component waveform data, from 11 Hi-net stations managed by the National Research Institute for Earth Science and Disaster Resilience (NIED; National Research Institute for Earth Science and Disaster Resilience 2019b), and one JMA station (Fig. 1). The time period for the data analysis was from March 1 to October 31, 2018.

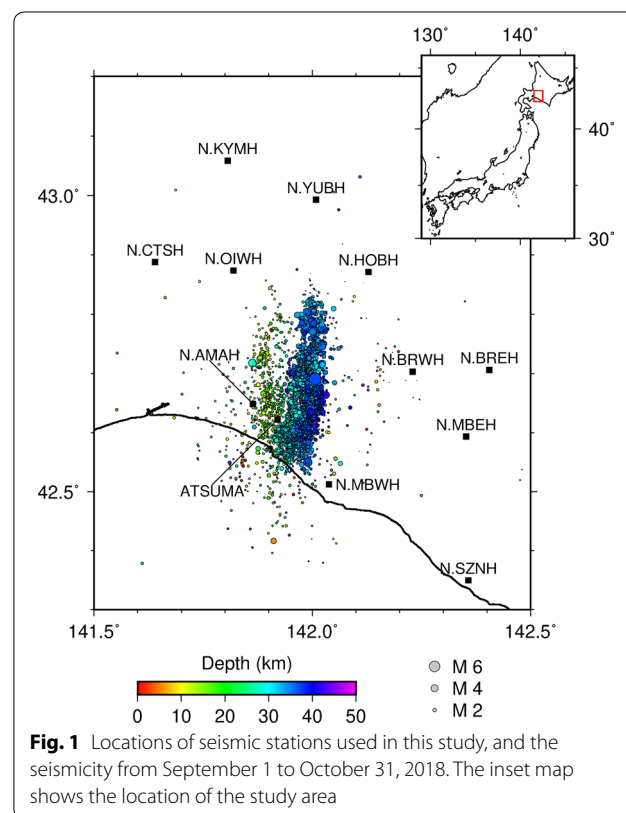


Fig. 1 Locations of seismic stations used in this study, and the seismicity from September 1 to October 31, 2018. The inset map shows the location of the study area

Calculating ACFs

We computed daily ACFs to detect temporal subsurface variations. Firstly, we divided 1-day records into 1-min time windows, with overlaps of 30 s; then, we applied a bandpass filter between 0.1–0.5 Hz, 1–3 Hz, and 2–8 Hz to the time-windowed data, after removing the linear trend and offset. We then carried out down-sampling from 100 to 20 Hz and one-bit normalization (after, e.g., Campillo and Paul 2003). We then computed ACFs for all time windows, and averaged them to obtain daily ACFs.

The computed daily ACFs in the 0.1–0.5 Hz and 2–8 Hz ranges were unstable, and in the 0.1–0.5 Hz range, temporal phase fluctuations of the ACFs were too large to detect subtle change due to subsurface structural variation, which may have been caused by temporal change in the distribution sources of microseisms. In the 1–3 Hz and 2–8 Hz ranges, some stations showed monotonic behavior, with peak frequencies above 3 Hz. Therefore, we again applied a bandpass filter, between 1 and 2 Hz, to the ACFs in the 1–3 Hz range, and to obtain more stable ACFs, we stacked the ACFs for 1 week before the corresponding dates.

Temporal changes in distribution sources of ambient noise have been reported as causing apparent changes to ACFs and in seismic velocity (Wegler et al. 2009). For detecting temporal changes in subsurface structure after large earthquakes, contamination of aftershocks in observed records may be the main factor changing the source distributions. Thus, we discarded the 1-min time windows containing earthquake signals, based on the standard deviation of the observed amplitude. We set threshold values as five times the median of the standard deviation during the whole observation period, and when standard deviations in a time window exceeded the thresholds, those time windows were not used to compute ACFs.

Stretching method

The stretching method was used to estimate velocity change (e.g., Sens-Schönfelder and Wegler 2006). The stretching method assumes a spatially homogeneous velocity change. With this assumption, the time delay after seismic velocity change can be predicted as shown in (1), where dv/v is a velocity change ratio, t is the lag time of the ACF, and dt is the time shift in the ACF at t .

$$dv/v = -dt/t \quad (1)$$

The ACF waveform is stretched or compressed by the predicted time delay and is then cross-correlated with a reference waveform. We can obtain the optimum value of dv/v by maximizing the cross-correlation coefficient between the stretched and reference ACFs. The reference

ACF in this study was calculated from the mean of all ACFs before the mainshock. We performed grid searches for dv/v within the range from -5 to 5% , with steps of 0.1% . Three lag time windows of 4–15 s, 4–9.5 s, and 9.5–15 s were examined. The dv/v measurement standard deviations were estimated using the following theoretical formula (Eq. (2) from Weaver et al. 2011). In (2), T is the inverse of the frequency band, t_1 and t_2 are the minimum value and the maximum value of the time window, respectively, ω_c is the median value of the frequency, and CC is the correlation coefficient between the reference ACF and other ACFs.

$$\sigma_d = \frac{\sqrt{1 - CC^2}}{2CC} \sqrt{\frac{6\sqrt{\frac{\pi}{2}}T}{\omega_c^2(t_2^3 - t_1^3)}} \quad (2)$$

Detecting waveform distortion

If the earthquake perturbs not only seismic velocity but also scattering property, by crack nucleation and/or fault zone damage, we can observe distortion of the ACF waveforms, in addition to the phase delay caused by velocity change. In order to quantify the waveform distortion, we compared averaged ACFs before and after the mainshock. We stretched or compressed the post-seismic ACF according to Eq. (1) and computed maximum correlation coefficients using moving time windows of 3 s, using 0.5-s steps. Waveform stretching corrects the phase delay due to seismic velocity change and thus enables detection of waveform distortion without phase shift. The moving time window allowed us to examine the relationship between lag time and waveform distortion.

Results

We detected changes to the ACFs after the mainshock. Figure 2 shows the calculated ACFs at seismic stations N.AMAH and ATSUMA: At N.AMAH, we found ACF phase delays at lag times 4–6 s after the mainshock, while at ATSUMA, we could also see ACF phase delays at lag times 4–9 s after the mainshock, and further confirmed the tendency of phase delay to increase with lag time. In addition to the phase delays, we found changes in the characteristics of the ACF waveform. The shape of the ACF waveform changed before and after the earthquake around lag times 6, 9, and 12 s, at N.AMAH, and around the lag time 10 s at ATSUMA. Around the lag times, simple homogeneous phase shifts based on Eq. (1) cannot explain the change in the ACF waveform.

The stretching method revealed the temporal changes to the dv/v at each station. Figure 3 shows the result of the stretching method with a time window of 4–15 s. The dv/v for all stations, except for N.KYMH, fluctuated within $\pm 0.5\%$ of the value recorded before the

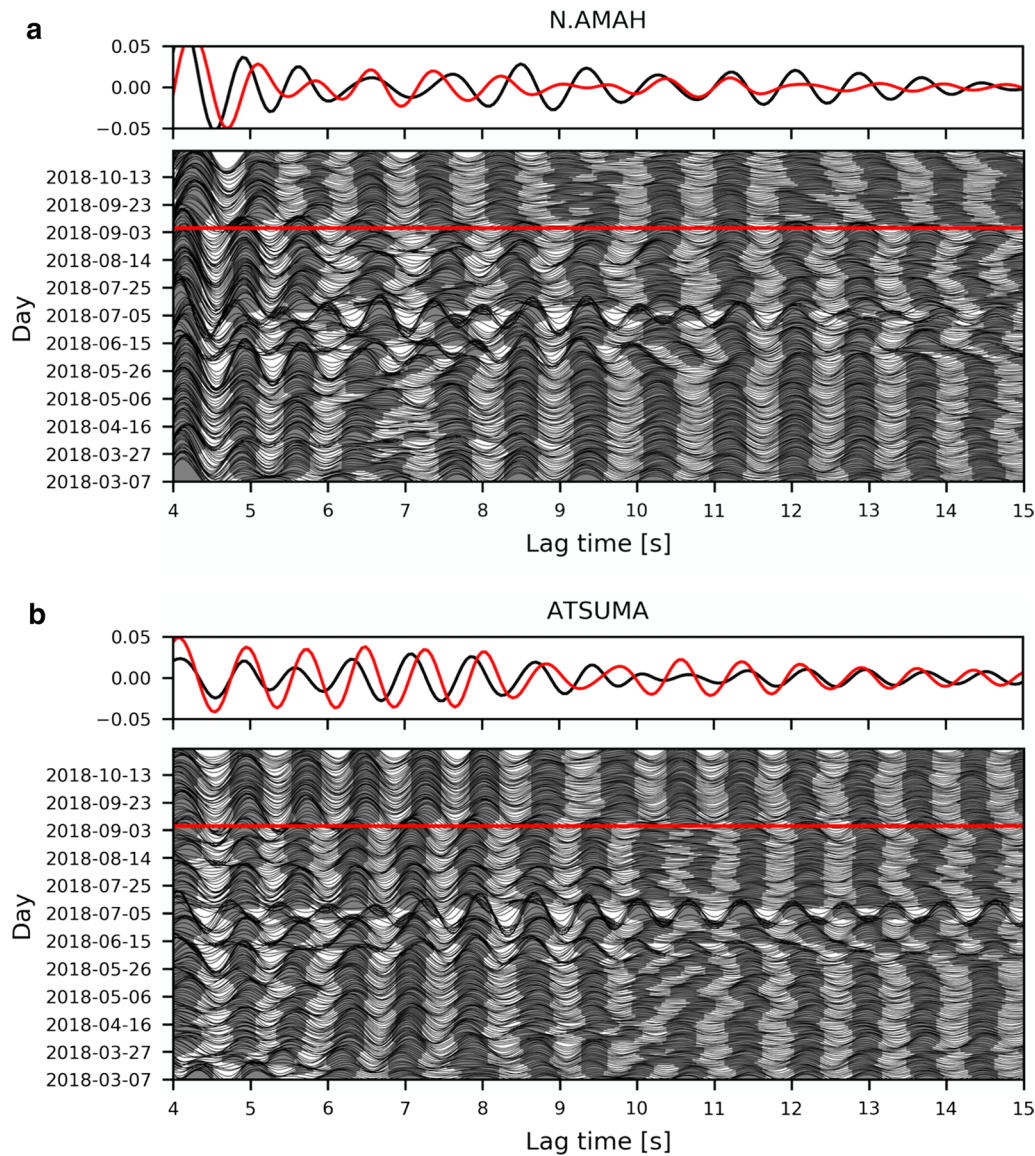
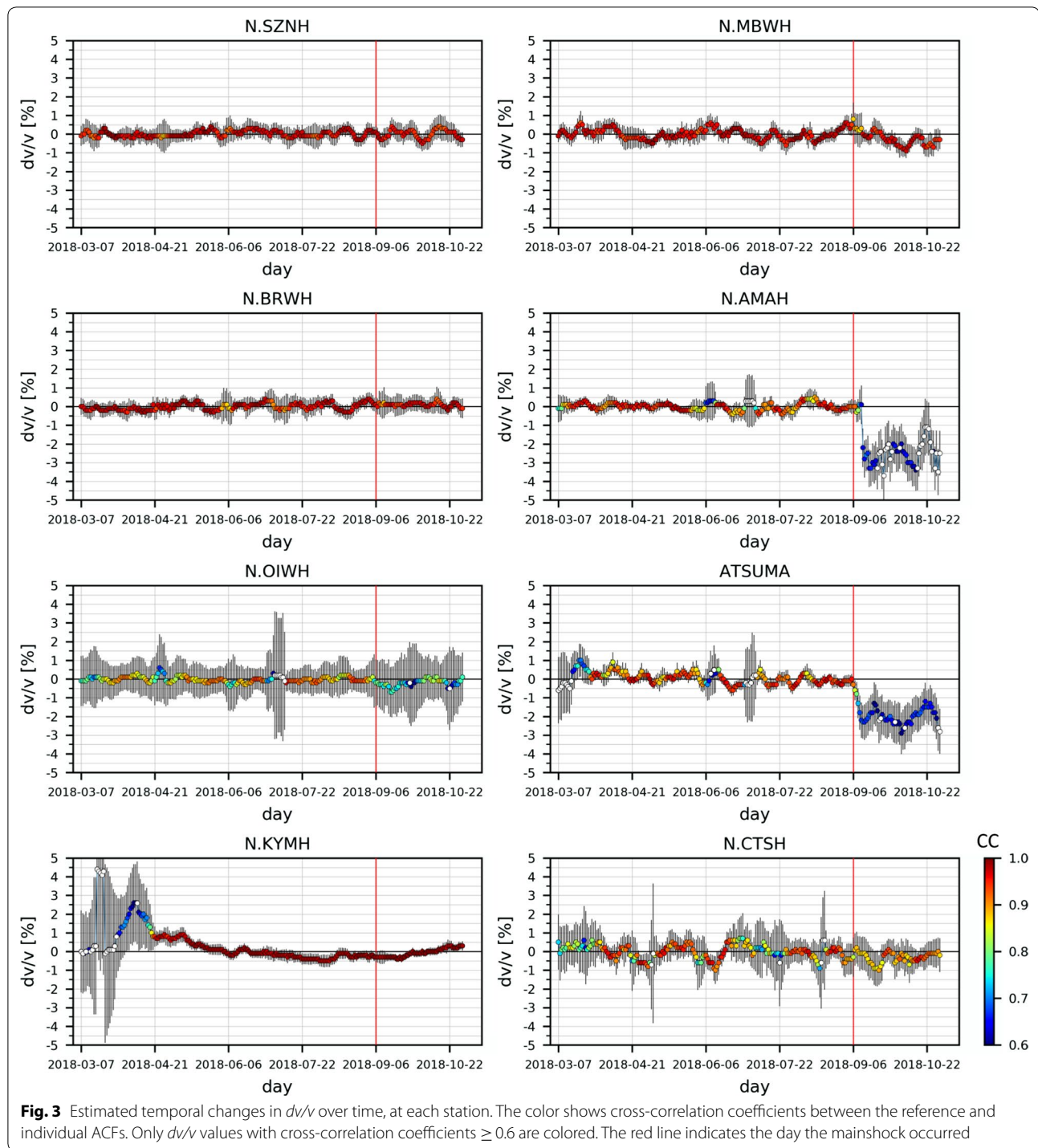


Fig. 2 Calculated ACFs at **a** N.AMAH, and **b** ATSUMA seismic stations. The top panels show the averaged ACFs before (black) and after (red) the mainshock. The bottom panels show the 7-day averages of the ACFs. The red line in the bottom panels indicates the day the mainshock occurred

earthquake. At N.AMAH, which was close to the main shock epicenter, the seismic velocity decreased by about 3% after the main shock. ATSUMA station also showed seismic velocity reduction, in this case by about 2%. Post-seismic dv/v recovery was not clear within the analysis period. Although a dv/v reduction exceeding 1% was not observed at other stations, the average values of the dv/v after the earthquake were smaller than the averages before the earthquake in N.MBWH, N.OIWH, and N.CTSH. In order to obtain the coseismic changes in dv/v , we averaged the dv/v after the mainshock in Fig. 3 using the errors of the individual

measurements as a weighting factor. The average values and standard deviations of the average are listed in Table 1, and most of the stations show coseismic velocity decreases.

Note that the 7-day averages of the ACFs before the corresponding dates were used to estimate the velocity changes. The 7-day moving average causes apparent time delay of the velocity change. In addition, data were missed just after the main shock for 2 days at N.AMAH and a half day at ATSUMA. The aftershock removal in the ACF also may reduce the available data soon after the mainshock. Although the velocity



reduction occurred a few days after the main shock at N.AMAH and gradually occurred at ATSUMA, the delayed response can be explained by the aforementioned factors.

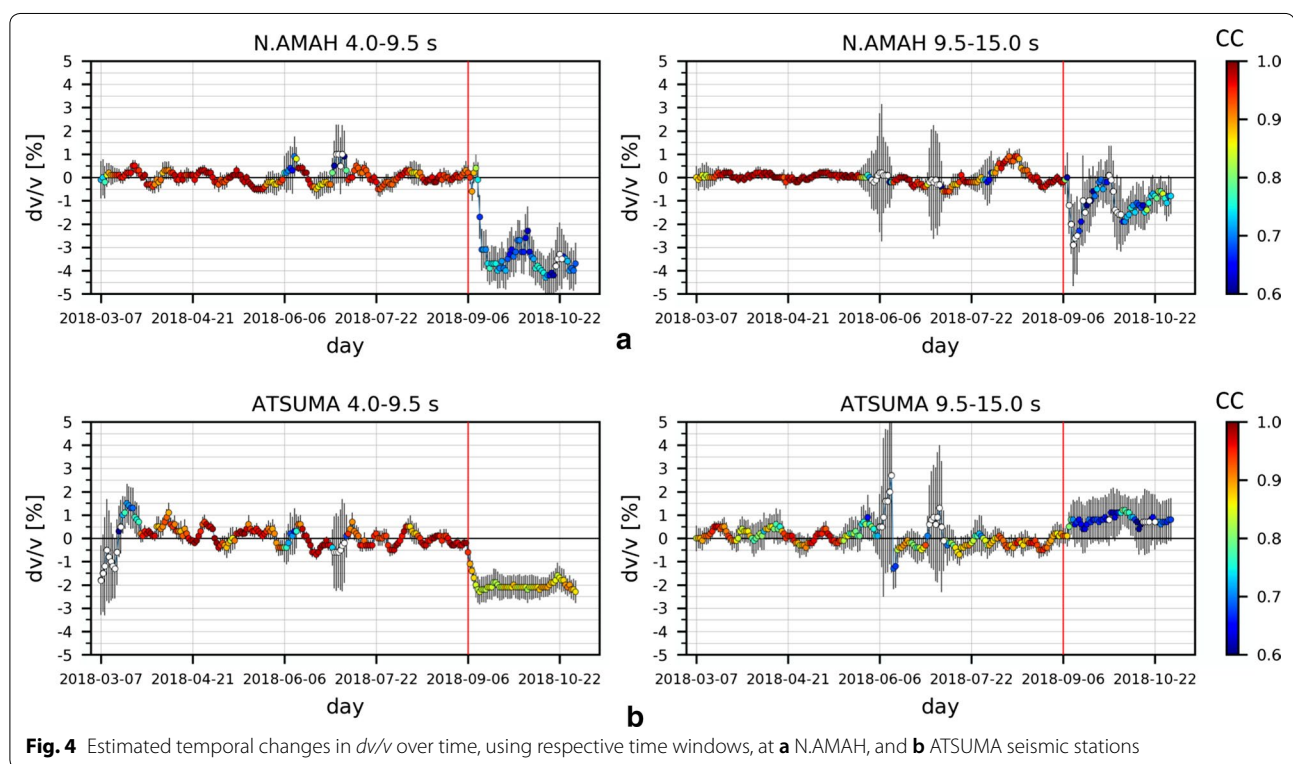
The results of the stretching method depended on the time window used. Figure 4a, b shows the results of the

stretching method, with the time windows 4–9.5 s and 9.5–15 s, at N.AMAH and ATSUMA, respectively. The magnitude of the dv/v differed when we used different time windows, which suggested that, at these two stations, the ACF changes could not be simply explained by a homogeneous velocity change. In addition, the

Table 1 Average values in dv/v and their standard deviations estimated from the three time windows, and computed indexes of strong ground motion, at each station

Station	4.0–15.0 s		4.0–9.5 s		9.5–15.0 s		Strong motion indexes			
	dv/v	Error	dv/v	Error	dv/v	Error	Vs30	PGA	PGV	PDS
	[%]	[%]	[%]	[%]	[%]	[%]	[m/s]	[gal]	[m/s]	[10 ⁻³]
N.AMAH*	-2.61	0.16	-3.58	0.27	-1.02	0.27	111	958.3	1.820	16.38
ATSUMA	-2.01	0.14	-2.06	0.15	0.84	0.29	N/A	N/A	N/A	N/A
N.MBWH	-0.33	0.06	-0.40	0.05	-0.15	0.23	341	587.7	0.636	1.86
N.CTSH	-0.31	0.10	-0.37	0.08	-0.28	0.21	326	275.5	0.318	0.98
N.YUBH	-0.28	0.02	-0.33	0.04	-0.14	0.07	1027	172.7	0.103	0.10
N.OIWH	-0.17	0.19	-0.02	0.19	-0.18	0.23	307	1928.2	2.637	8.59
N.HOBH	-0.13	0.02	-0.21	0.03	0.02	0.08	542	775.3	0.364	0.67
N.KYMH	-0.08	0.03	-0.07	0.03	-0.08	0.04	267	770.5	0.348	1.30
N.MBEH	-0.07	0.03	-0.06	0.04	-0.14	0.09	341	456.4	0.236	0.69
N.SZNH	-0.02	0.07	0.04	0.07	-0.13	0.14	412	255.8	0.342	0.83
N.BREH	0.01	0.03	0.07	0.04	-0.08	0.09	444	319.7	0.230	0.52
N.BRWH*	0.07	0.06	0.12	0.05	-0.02	0.14	368	889.6	0.956	2.60

*Indicates we used unscreened data from KiK-net



correlation coefficient after the waveform stretching decreased after the earthquake (Figs. 3 and 4). This decoherence also suggested that not only seismic velocity, but also scattering properties, affected temporal ACF variation.

Figure 5 shows the lag time dependency of the ACF waveform change, based on the correlation coefficient between the reference and post-seismic ACFs. The degradation characteristics of the correlation coefficient varied between seismic stations: It was seen to decrease

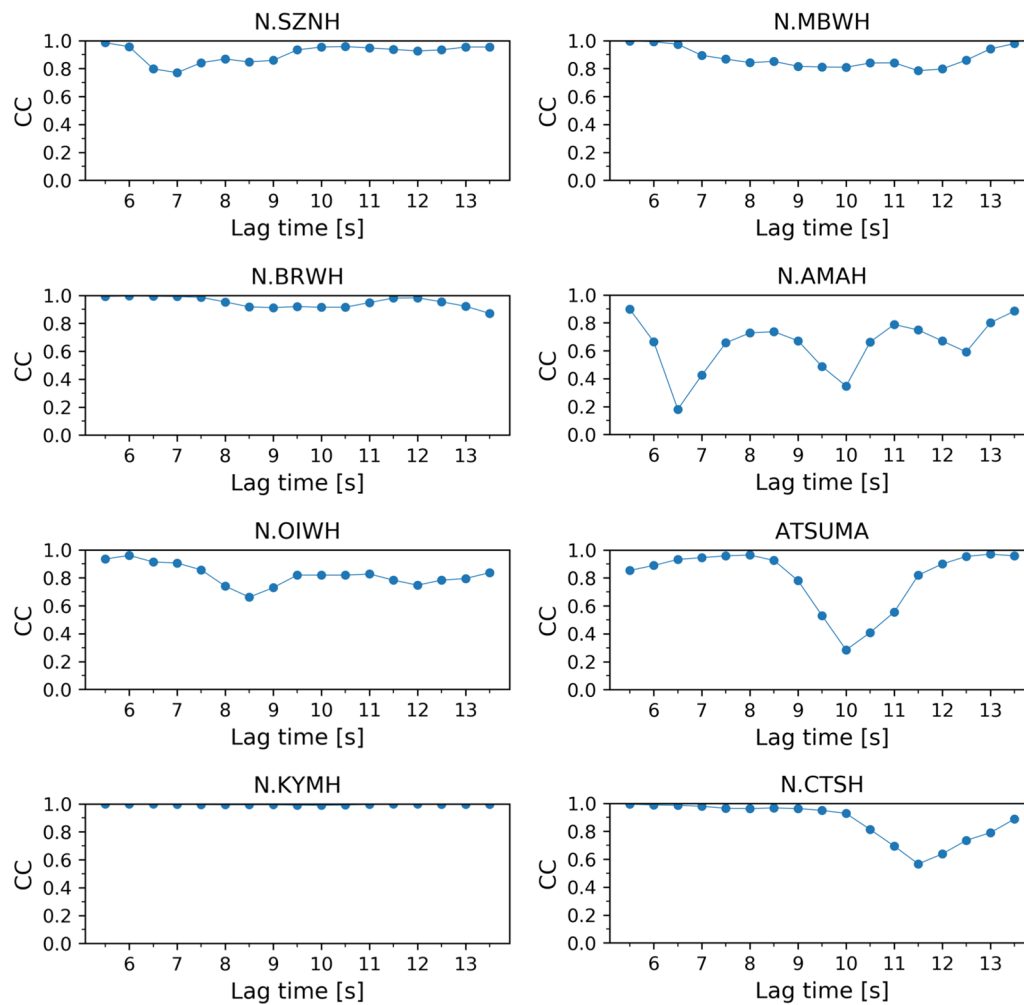


Fig. 5 The relationship between cross-correlation coefficients and lag times for each station

significantly near the lag time of 10 s, at ATSUMA, and around 6.5 s, 10 s, and 12.5 s, at N.AMAH. The decrease in correlation values could also be confirmed from the ACFs shown in Fig. 2. In general, later lag times may have tended to have low correlation coefficients, due to a decreasing signal-to-noise ratio with increasing lag time. At ATSUMA station however, for example, the correlation coefficient became higher than 0.9, after the drop in the correlation coefficient around 10 s. Thus, the decreased correlation values have reflected changes to the subsurface structure.

Discussion

The reduction of $d\nu/\nu$ after the mainshock

Immediately after the mainshock on September 6, the $d\nu/\nu$ was recorded to decrease by 2–3%, at two seismic stations close to the mainshock. Previous studies reported similar coseismic reductions, of $d\nu/\nu$ by a few

percent, at the focal region of large earthquakes (e.g., Hobiger et al. 2016). The frequency dependence of $d\nu/\nu$, and comparisons with vertical seismic array analyses, have indicated that such velocity reductions appear to concentrate in the shallow subsurface area, up to a few hundred meters deep (Hobiger et al. 2014; Takagi et al. 2012). Larger velocity decreases in the time window of 4.0–9.5 s than that of 9.5–15.0 s also imply that velocity decrease is mainly located in the shallow subsurface (Table 1). Thus, the $d\nu/\nu$ decreases in the ACF estimated by the present study may be due to the shallow ground damage caused by strong ground motions.

We compared the observed seismic velocity change with indexes of strong ground motion. Table 1 shows V_{s30} at each station, peak ground acceleration (PGA), peak ground velocity (PGV), and peak dynamic strain (PDS), caused by the strong motion of the mainshock. V_{s30} is the average S-wave velocity from the ground surface to 30 m

and is defined as shown by Eq. (3), where d_i is the thickness of a layer and v_{s_i} is its S-wave velocity.

$$V_{s30} = \frac{30 [\text{m}]}{\sum_i (d_i/v_{s_i})} \quad (3)$$

We estimated PGA and PGV using strong motion records on the ground surface from KiK-net stations collocated with Hi-net stations (National Research Institute for Earth Science and Disaster Resilience 2019a). PDS is the maximum value of a dynamic strain change due to strong ground motion, which is estimated by dividing PGV by V_{s30} (Takagi and Okada 2012; Sawazaki and Snieder 2013). The station with the maximum PGA and PGV, N.OIWA, showed a dv/v decrease of 0.17%. N.AMAH, on the other hand, had smaller PGA and PGV than those of N.OIWA, with the PDS a maximum at N.AMAH. The maximum coseismic decrease in dv/v was 2.61% among these stations and observed at N.AMAH, indicating that there may be a better relationship between dv/v and PDS, as opposed to PGA and PGV. Moreover, the velocity drop with a similar magnitude to previous works, and correlation with PDS, implied that damage in the shallow layers due to strong ground motion was the main cause of the velocity drop.

Hobiger et al. (2016) measured seismic velocity changes accompanying multiple, large earthquakes in Japan, and compared these with several indexes of strong motion. The data shown in Table 1 were consistent with the relationship trend between the seismic velocity changes and strong motion indexes that they estimated. However, since there is no simple linear relationship between PDS and the rate of dv/v , it is difficult to explain velocity changes using only PDS. For example, as suggested by the data from N.MBWH, N.CTSH, N.YUBH, N.OIWA, N.HOBH stations, although PDS values differed by almost one order of magnitude, their dv/v was the same degree, which suggested that susceptibility to velocity change varied with the ground and geological structure (Brennguier et al. 2014).

Degradation of waveform correlation

We examined the relationship between the lag times and correlation coefficients and found decreased waveform correlations before and after the mainshock. Such decorrelation of the ACF waveforms could be attributed to the changed subsurface scattering property.

Another possible cause of the ACF waveform decorrelation is spatially inhomogeneous or localized velocity changes. Because we assumed spatially homogeneous velocity changes and thus homogeneous phase shifts of the ACFs in 3-s time windows, inhomogeneous phase shifts caused by inhomogeneous or localized velocity changes

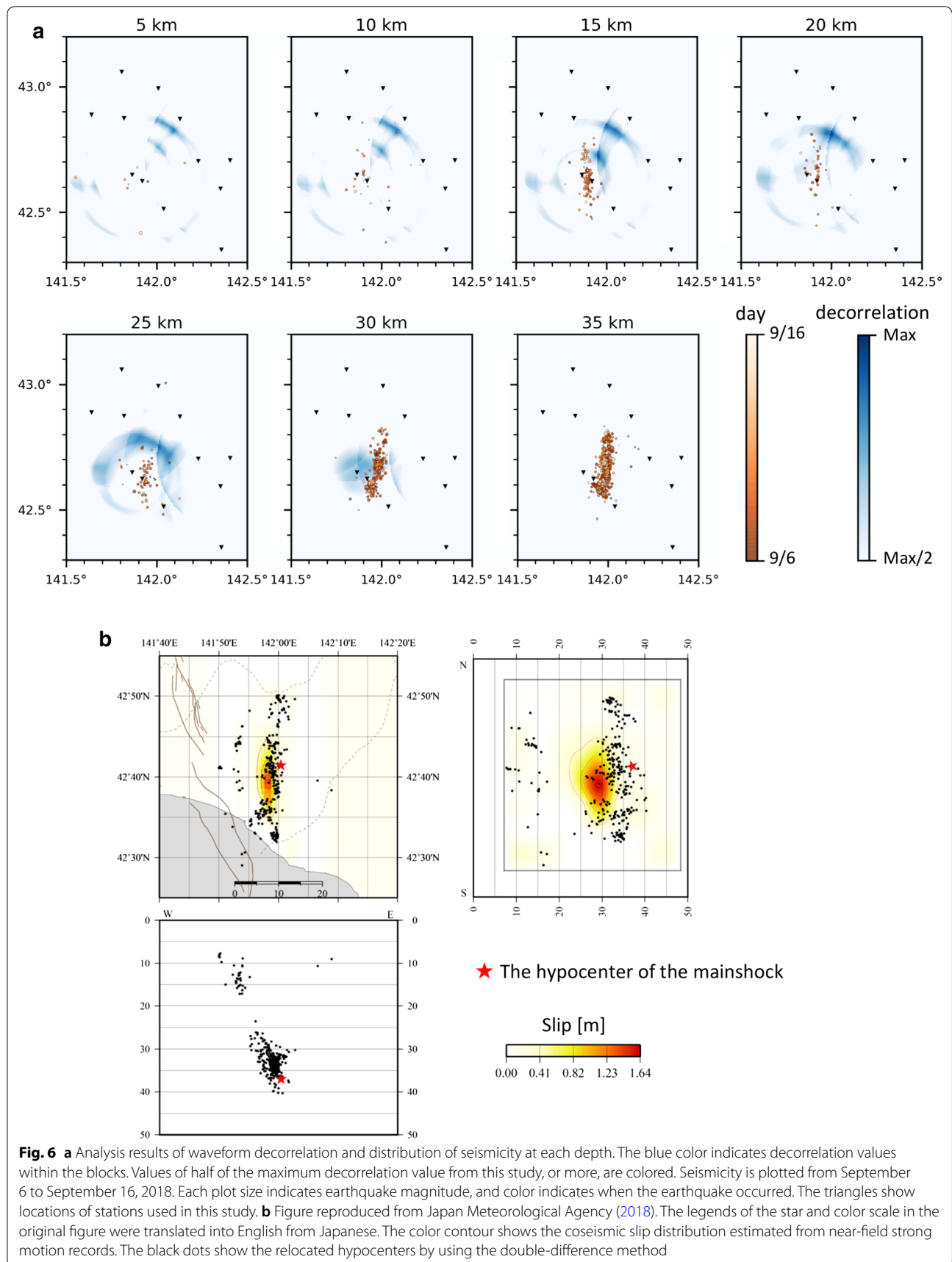
may result in the decorrelation of the ACF waveforms. For example, the ACFs of N.AMAH station show the phase delays in 4–6 s and phase advances in 7–9 s, the latter of which may be interpreted as localized velocity increase. Although such localized velocity changes may partly explain the observed decorrelation, the shapes and amplitudes of the ACFs around 10 s at ATSUMA, and around 9 s and later lag times at N.AMAH do not appear to be explained by inhomogeneous phase shifts. Thus, hereafter, we attribute the decorrelation to the scattering property changes and discuss the location of the changes.

In order to locate the area showing scattering property change, we needed to distinguish the dominant ACF wave type. Obermann et al. (2013) showed that the body wave component dominated the surface wave in the latter part of CCF. Generally, it has been suggested that surface waves and body waves were included in the ambient noise of 1 Hz or more (Bonnefoy-Claudet et al. 2006). Takagi (2014) showed that the power spectral ratio of Rayleigh waves and P-waves approached 1, in the ACF of 1–2 Hz, vertical component, ambient noise. Roux et al. (2005) also showed that Rayleigh waves and P-waves were extracted from the CCF of ambient noise vertical components and that P-waves were dominant at 0.7 Hz and above.

Since the possibility of the contribution of the surface wave cannot be completely excluded, by virtue of this research alone, it will be necessary to clarify the ACF wave field, by using, for example, dense array observations near the station where the change was detected. However, according to the previous studies noted above, it may be reasonable to assume that degradation of the waveform correlation was due to P-waves.

In order to locate the area that corresponded with the waveform correlation degradation, we carried out the following analysis. First, we divided the target area into 0.5-km side cubic blocks and computed the two-way travel times from the seismic stations to cubic blocks. A one-dimensional (1D) JMA velocity structure was used for ray tracing (Ueno et al. 2002)—and note that we used the same 1D velocity structure as was used for hypocenter location by the JMA. Then, assuming that the ACFs comprised single backscattered P-waves, and thus regarding the lag times of the ACFs as the two-way travel times, we assigned the decorrelation values ($1 - CC$) of the corresponding lag times to the cubic blocks. We obtained spatial distribution of the decorrelation values by summing the contributions from all station used in this study. The larger the value of decorrelation, the more significant the influence on the waveform change.

We found three areas with large decorrelation values, as shown in Fig. 6a, which were therefore the candidate



regions for scattering property changes. Two areas were located near the northern edge of the aftershock distribution. The depths of the maximum values were 15 and 20 km, although they spread in the depth direction. The other area with large decorrelation value was located at 30 km depth, just west of the central part of the aftershock distribution. Since the average P-wave velocity was approximately 6.0 km/s, the large decorrelation area reflected correlation reductions of about 10 s, at N.AMAH and ATSUMA.

Figure 6b shows the coseismic slip distribution estimated from strong motion records and hypocenters relocated by applying the double-difference method (Japan Meteorological Agency 2018). The aftershocks were distributed in two, separated depth ranges of the fault plane: 10–15 km and 30–40 km. The coseismic slips were estimated between the two aftershock clusters. The maximum slip was located at 30 km, just above the central part of the deeper aftershock cluster. Geodetic data also suggested that the coseismic fault was modeled at 15–30 km (Geospatial Information Authority of Japan 2018). We found that the large decorrelation areas were located at the depth of 15–30 km. It is noteworthy that one large decorrelation areas, at 30 km, was close to the location of the maximum slip area. The spatial correlation suggested that the decreased ACF waveform correlation in this study was related to coseismic slip on the fault. One interpretation is that the coseismic fault rupture generated cracks within or around the fault zone and that this changed the scattering property, or scatterer distribution.

Conclusion

In the focal region of the 2018 Hokkaido Eastern Iwate Earthquake, we detected temporal changes in seismic velocity and scattering property, based on autocorrelation analysis of ambient seismic noise. The stretching method, with the lag time window of 4.0–9.5 s, estimated seismic velocity reductions of 2–3% at two stations close to the epicenter. Coseismic velocity drops of similar magnitude (a few percent) have been previously reported in the shallow subsurface, down to a few hundred meters. Based on the relation between the values of PGA, PGV, and PDS, and the $d\nu/\nu$, we showed that the velocity change was more closely related to PDS, than to PGA or PGV. The amplitude of the velocity drop, and correlation with PDS, implied that damage in the shallow layer due to strong ground motion was the main cause of the velocity drop.

We also detected waveform distortion of ACFs, before and after the mainshock. If the ACFs were composed of single, backscattered P-waves, the change in scattering property could be estimated where the maximum

slip was estimated. This suggested that the coseismic fault rupture generated cracks around the fault, which changed the scattering property in and around the fault zone.

Abbreviations

ACF: autocorrelation function; CCF: cross-correlation function; JMA: Japan Meteorological Agency; NIED: National Research Institute for Earth Science and Disaster Resilience; PGA: peak ground acceleration; PGV: peak ground velocity; PDS: peak dynamic strain.

Acknowledgements

We used waveform data from seismic stations maintained by JMA and also used waveform data from Hi-net and KIK-net, maintained by NIED. Figure 6b is a reproduction of a figure made by JMA in the report of the Headquarters for Earthquake Research Promotion. We thank JMA and the Headquarters for Earthquake Research Promotion for the reuse permission. We plotted a figure using Genetic Mapping Tools (Wessel et al. 2013). We would like to thank Editage (www.editage.jp) for English language editing. We thank Editor Saeko Kita, Takuto Maeda, and an anonymous reviewer for their constructive comments.

Authors' contributions

HI performed data analysis and prepared the manuscript. RT helped with interpretation and revised the manuscript. Both authors read and approved the final manuscript.

Funding

This study was supported by the Ministry of Education, Culture, Sports, Science and Technology (MEXT) of Japan, under its Earthquake and Volcano Hazards Observation and Research Program. This research was also supported by JSPS KAKENHI Grant Numbers 16K17788, 17H02950, and 18K19952.

Availability of data and materials

The continuous seismic waveform data are available via the web site of NIED (<https://hinetwww11.bosai.go.jp/auth/?LANG=en>).

Competing interests

The authors declare that they have no competing interests.

Author details

¹ Research Center for Prediction of Earthquakes and Volcanic Eruptions, Graduate School of Science, Tohoku University, 6-6 Aza-Aoba, Aramaki, Aoba-ku, Sendai 980-8578, Japan. ² Present Address: LAC Co., Ltd, 2-16-1 Hirakawacho, Chiyoda-ku, Tokyo 102-0093, Japan.

Received: 24 February 2019 Accepted: 18 June 2019

Published online: 27 June 2019

References

- Bonnefoy-Claudet S, Cornou C, Bard PY, Cotton F, Moczo P, Kristek J, Fah D (2006) H/V ratio: a tool for site effects evaluation. Results from 1-D noise simulations. *Geophys J Int* 167:827–837. <https://doi.org/10.1111/j.1365-246X.2006.03154.x>
- Brenguier F, Campillo M, Hadziioannou C, Shapiro NM, Nadeau RM, Larose E (2008) Postseismic relaxation along the San Andreas fault at parkfield from continuous seismological observations. *Science* 321(5895):1478–1481. <https://doi.org/10.1126/science.1160943>
- Brenguier F, Campillo M, Takeda T, Aoki Y, Shapiro NM, Briand X, Emoto K, Miyake H (2014) Mapping pressurized volcanic fluids from induced crustal seismic velocity drops. *Science* 345(6192):80–82. <https://doi.org/10.1126/science.1254073>
- Campillo M, Paul A (2003) Long-range correlations in the diffuse seismic coda. *Science* 299(5606):547–549. <https://doi.org/10.1126/science.1078551>
- Chen JH, Froment B, Liu QY, Campillo M (2010) Distribution of seismic wave speed changes associated with the 12 May 2008 Mw 7.9 Wenchuan

- earthquake. *Geophys Res Lett* 37:L18302. <https://doi.org/10.1029/2010GL044582>
- Chen KH, Furumura T, Rubinstein J (2015) Near-surface versus fault zone damage following the 1999 Chi-Chi earthquake: observation and simulation of repeating earthquakes. *J Geophys Res Solid Earth* 120:2426–2445. <https://doi.org/10.1002/2014JB011719>
- Geospatial Information Authority of Japan (2018) Information of the 2018 Hokkaido Eastern Iburi earthquake. <http://www.gsi.go.jp/BOUSAI/H30-hokkaidoiburi-east-earthquake-index.html#8>. Accessed 9 Jan 2019
- Hobiger M, Wegler U, Shiomi K, Nakahara H (2014) Single-station cross-correlation analysis of ambient seismic noise: application to stations in the surroundings of the 2008 Iwate–Miyagi Nairiku earthquake. *Geophys J Int* 198:90–109. <https://doi.org/10.1093/gji/ggu115>
- Hobiger M, Wegler U, Shiomi K, Nakahara H (2016) Coseismic and post-seismic velocity changes detected by passive image interferometry: comparison of one great and five strong earthquakes in Japan. *Geophys J Int* 205:1053–1073. <https://doi.org/10.1093/gji/ggw066>
- Japan Meteorological Agency (2018) The 2018 Hokkaido Eastern Iburi earthquake (Relocated hypocenter distribution by using the DD method). Evaluation of the 2018 Hokkaido Eastern Iburi earthquake (Published on 12 October 2018). https://www.static.jishin.go.jp/resource/monthly/2018/20180906_iburi_3.pdf. Accessed 9 Jan 2019
- Katsumata A (2010) Depth of the Moho discontinuity beneath the Japanese islands estimated by traveltime analysis. *J Geophys Res* 115:B04303. <https://doi.org/10.1029/2008JB005864>
- Kita S, Okada T, Hasegawa A, Nakajima J, Matsuzawa T (2010) Anomalous deepening of a seismic belt in the upper-plane of the double seismic zone in the Pacific slab beneath the Hokkaido corner: possible evidence for thermal shielding caused by subducted forearc crust materials. *Earth Planet Sci Lett* 290:415–426. <https://doi.org/10.1016/j.epsl.2009.12.038>
- Kita S, Hasegawa A, Nakajima J, Okada T, Matsuzawa T, Katsumata K (2012) High-resolution seismic velocity structure beneath the Hokkaido corner, northern Japan: Arc-arc collision and origins of the 1970M 6.7 Hidaka and 1982M 7.1 Urakawa-oki earthquakes. *J Geophys Res* 117:B12301. <https://doi.org/10.1029/2012jb009356>
- Maeda T, Obara K, Yukutake Y (2010) Seismic velocity decrease and recovery related to earthquake swarms in a geothermal area. *Earth Planets Space* 62(9):685–691. <https://doi.org/10.5047/eps.2010.08.006>
- Nakata N, Snieder R (2011) Near-surface weakening in Japan after the 2011 Tohoku-Oki earthquake. *Geophys Res Lett* 38:L17302. <https://doi.org/10.1029/2011GL048800>
- National Research Institute for Earth Science and Disaster Resilience (2018) The 6 September 2018 earthquake in the center-eastern Iburi district: hypocenter distribution and first motion focal mechanism. <http://www.hinet.bosai.go.jp/topics/ishikari180906/?LANG=ja&m=summary>. Accessed 14 Feb 2019
- National Research Institute for Earth Science and Disaster Resilience (2019a) NIED K-NET, KiK-net. National Research Institute for Earth Science and Disaster Resilience, Tsukuba. <https://doi.org/10.17598/NIED.0004>
- National Research Institute for Earth Science and Disaster Resilience (2019b) NIED Hi-net. National Research Institute for Earth Science and Disaster Resilience, Tsukuba. <https://doi.org/10.17598/nied.0003>
- Nishimura T, Nakamachi H, Tanaka S, Sato M, Kobayashi T, Ueki S, Hama-guchi H, Ohtake M, Sato H (2000) Source process of very long period seismic events associated with the 1998 activity of Iwate Volcano, northeastern Japan. *J Geophys Res* 105(B8):19135–19147. <https://doi.org/10.1029/2000JB900155>
- Obermann A, Planes T, Larose E, Sens-Schönfelder C, Campillo M (2013) Depth sensitivity of seismic coda waves to velocity perturbations in an elastic heterogeneous medium. *Geophys J Int* 1:11. <https://doi.org/10.1093/gji/ggt043>
- Obermann A, Froment B, Campillo M, Larose E, Planes T, Valette B, Chen JH, Liu QY (2014) Seismic noise correlations to image structural and mechanical changes associated with the Mw 7.9 2008 Wenchuan earthquake. *J Geophys Res* 119:3155–3168. <https://doi.org/10.1002/2013JB010932>
- Poupinet G, Ellsworth WL, Frechet J (1984) Monitoring velocity variations in the crust using earthquake doublets: an application to the Calaveras fault, California. *J Geophys Res* 89(B7):5719–5731
- Rivet D, Campillo M, Shapiro NM, Cruz-Atienza V, Radigue M, Cotte N, Kostoglodov V (2011) Seismic evidence of nonlinear crustal deformation during a large slow slip event in Mexico. *Geophys Res Lett* 38:L08308. <https://doi.org/10.1029/2011GL047151>
- Roux P, Sabra KG, Gerstoft P, Kuperman WA (2005) P-waves from cross-correlation of seismic noise. *Geophys Res Lett* 32:L19303. <https://doi.org/10.1029/2005GL023803>
- Sawazaki K, Snieder R (2013) Time-lapse changes of P- and S-wave velocities and shear wave splitting in the first year after the 2011 Tohoku earthquake, Japan: shallow subsurface. *Geophys J Int* 193:238–251. <https://doi.org/10.1093/gji/ggs080>
- Sens-Schönfelder C, Wegler U (2006) Passive image interferometry and seasonal variations of seismic velocities at Merapi Volcano, Indonesia. *Geophys Res Lett* 33:L21302. <https://doi.org/10.1029/2006GL027797>
- Takagi R (2014) Development in seismic interferometry for subsurface monitoring—an application to the 2011 Tohoku-oki earthquake. Ph.D. thesis, Department of Geophysics, Graduate School of Science, Tohoku University
- Takagi R, Okada T (2012) Temporal change in shear velocity and polarization anisotropy related to the 2011 M9.0 Tohoku-Oki earthquake examined using KiK-net vertical array data. *Geophys Res Lett* 39:L09310. <https://doi.org/10.1029/2012gl051342>
- Takagi R, Okada T, Nakahara H, Umino N, Hasegawa A (2012) Coseismic velocity change in and around the focal region of the 2008 Iwate–Miyagi Nairiku earthquake. *J Geophys Res* 117:B06315. <https://doi.org/10.1029/2012JB009252>
- Ueno H, Hatakeyama S, Aketagawa T, Funasaki J, Hamada N (2002) Improvement of hypocenter determination procedures in the Japan Meteorological Agency (in Japanese with English abstract). *Q J Seismol* 65:123–134
- Ueno T, Saito T, Shiomi K, Enescu B, Hirose H, Obara K (2012) Fractional seismic velocity change related to magma intrusions during earthquake swarms in the eastern Izu peninsula, central Japan. *J Geophys Res* 117:B12305. <https://doi.org/10.1029/2012JB009580>
- Weaver RL, Hadziioannou C, Larose E, Campillo M (2011) On the precision of noise correlation interferometry. *Geophys J Int* 168(3):1029–1033. <https://doi.org/10.1111/j.1365-246X.2011.05015.x>
- Wegler U, Nakahara H, Sens-Schönfelder C, Korn M, Shiomi K (2009) Sudden drop of seismic velocity after the 2004 Mw 6.6 mid-Niigata earthquake, Japan, observed with passive image interferometry. *J Geophys Res* 114:B06305. <https://doi.org/10.1029/2008jb005869>
- Wessel P, Smith WHF, Scharroo R, Luis J, Wobbe F (2013) Generic mapping tools: improved version released. *Eos Trans Am Geophys Union* 94(45):409–410
- Yukutake Y, Ueno T, Miyaoka K (2016) Determination of temporal changes in seismic velocity caused by volcanic activity in and around Hakone volcano, central Japan, using ambient seismic noise records. *Progr Earth Planet Sci* 3:29. <https://doi.org/10.1186/s40645-016-0106-5>

Publisher's Note

Springer Nature remains neutral with regard to jurisdictional claims in published maps and institutional affiliations.